Spectrochimica Acta Part A: Molecular and Biomolecular Spectroscopy, Volume 63, Issue 5, April 2006, Pages 929-939.

Modelling and interpretation of gas detection using remote laser pointers

J Hodgkinson [ac]*, B van Well[b], M Padgett[b] and R D Pride [ad]

a Advantica, Loughborough, UK
b Dept of Physics and Astronomy, Glasgow University, Glasgow, UK
c Now at School of Engineering, Cranfield University, Bedfordshire, MK 43 0AL, UK.
Address for correspondence.
Tel +44 (0) 1234 750111 ext 5364
Fax +44 (0) 1234 752452
j.hodgkinson@cranfield.ac.uk
d Now at Joint Research Centre, European Commission, Ispra, Italy

Abstract

We have developed a quantitative model of the performance of laser pointer style gas leak detectors, which are based on remote detection of backscattered radiation. The model incorporates instrumental noise limits, the reflectivity of the target background surface and a mathematical description of gas leak dispersion in constant wind speed and turbulence conditions. We have investigated optimum instrument performance and limits of detection in simulated leak detection situations. We predict that the optimum height for instruments is at eye level or above, giving an operating range of 10m or more for most background surfaces, in wind speeds of up to 2.5 $m.s^{-1}$. For ground based leak sources, we find laser pointer measurements are dominated by gas concentrations over a short distance close to the target surface, making their readings intuitive to end users in most cases. This finding is consistent with the results of field trials.

Keywords:
Gas, methane, leak, detection, dispersion

1 Introduction

There is great interest in remote gas detectors, based on tunable diode lasers, operating over distances of 10m or more[1,2,3]. These systems use a laser beam aimed through open space at a target, collecting the backscattered light and applying a spectroscopic signal demodulation. Applications include the detection of natural gas leaks from low-pressure distribution pipes, with a methane detector based on a tunable DFB laser emitting light at 1.65nm.

This detection geometry represents a significant step change within the gas industry from the use of pumped sampling sensors that detect gas concentrations at a single point in space. The new instruments present challenges for instrument designers and operators that cannot be fully addressed without also understanding the behaviour of the leaking gas plume. Iseki et al have modelled their system's reflectivity and noise performance, relating this to a minimum detectable gas concentration signals in ppm.m[1]. For indoor leaks in the absence of wind, they have demonstrated gas leak detection with leak rates as low as 0.01litre min^{-1}. We have now extended this understanding to include outdoor wind speed and turbulence characteristics as well as the effects of different leak plume viewing conditions.

We present results from a collaborative project to develop a laser pointer instrument. Understanding the interaction between the laser beam and the leaking gas needed to inform both instrument design and operation guidelines. Our model combines the behaviour of the dispersing gas plume, the background target, and the interaction of the instrument laser beam with both of these. It has enabled us to investigate trends in behaviour under controlled conditions, more rapidly than would be the case when performing field tests. We report our findings concerning the optimum instrument height, pointing accuracy required, ability to "zero trace" (confirm the absence of gas) and the intuitive use of the measurements to locate gas leaks. Conclusions drawn from the model have been compared qualitatively with the results of instrument field tests.

2 Method

A typical laser pointer, shown schematically in Figure 1, provides readings proportional to the number density of methane molecules along the path of the laser beam. Because the measurement takes the form of a line integral, the units of measurement are ppm.m as opposed to ppm, typically found with

traditional point sampling instruments. In other words, the instrument would give the same reading for (i) 100% gas spread over a distance of 1mm, and (ii) 1000ppm gas spread over a distance of 1m.

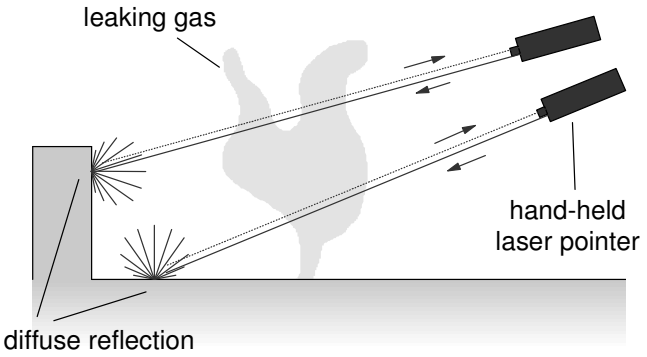

Figure 1. Schematic diagram of a laser pointer in action.

We used a Gaussian model of leaking gas concentrations, based on a previous study of gas dispersion performed using a wind tunnel. A computer model of the instrument response was developed, taking a line integral of gas concentrations through the simulated cloud from the position of the instrument to a target position on the ground. The relative positions of instrument and target could be changed in the model in three dimensions, as could the type of background target (using their different characteristic reflectivities). The line integral was summed numerically. Signal to noise ratios were considered using a model for surface reflectivity based on experimental data.

2.1 Gas dispersion model

As shown in Figure 2, a narrow plume may meander within a diffusely defined envelope, with a gas concentration that can change both spatially and temporally. The concentration map described by the following model should therefore be thought of as a gas probability distribution rather than as an instantaneous map of the gas concentration.

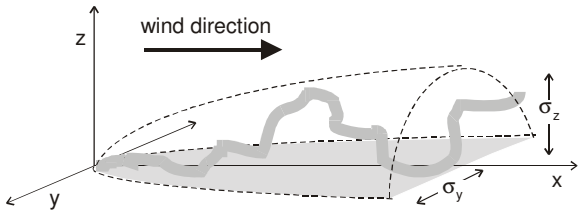

Figure 2. Schematic of a gas leak plume meandering within an envelope.

In the Pasquill-Gifford model for passive gas releases, the concentration of gas downwind of a ground level, point leak source at the origin (x,y,z) = (0,0,0) is predicted by the following Gaussian relationship[4].

$$C(x,y,z) = \frac{2Q}{\pi \sigma_y \sigma_z u} \exp\left[-\frac{1}{2}\left(\frac{y^2}{\sigma_y^2} + \frac{z^2}{\sigma_z^2}\right)\right] \quad (1)$$

C is the concentration in $kg \cdot m^{-3}$, Q is the flow rate in $kg \cdot s^{-1}$, σ_y and σ_z are dispersion coefficients in m, x, y and z are distances in m and u is the wind speed in $m \cdot s^{-1}$. For an extended source of width $2a$ along the y-axis, equation *(1)* is integrated over the source:

$$C(x,y,z) = \frac{Q}{\sqrt{2\pi}\,\sigma_z\, u\, a} \exp\left(-\frac{1}{2}\frac{z^2}{\sigma_z^2}\right)\left\{erf\left(\frac{1}{\sqrt{2}}\frac{(a-y)}{\sigma_y}\right) + erf\left(\frac{1}{\sqrt{2}}\frac{(a+y)}{\sigma_y}\right)\right\} \quad (2)$$

Ideally we would also integrate equation (2) over the extended source along the x-axis. However, the dependence of the dispersion coefficients, σ_y and σ_z, on x make this analytically difficult. Instead we have used equation (2) as it stands, making the approximation to our real rectangular source. At wind speeds of $\geq 1 m \cdot s^{-1}$ along the x-axis, downwind dispersion over the short (10cm) length of the source would be negligible.

The values of the gas dispersion coefficients σ_y and σ_z shown in equation (2) were found in a study of gas leak behaviour conducted in the controlled conditions of a wind tunnel[5]. Their values are dependent on the prevailing turbulence conditions, which in the wind tunnel were controlled so as to be representative of mixed rural setting (ie relatively flat, fields broken by hedges and occasional buildings). The more turbulent urban environment would necessitate use of different coefficients. So although these values are not universally applicable, we can nevertheless study trends and the question of the intuitiveness for our modelled instrument.

Table 1. Values of σ_y and σ_z used in this study for each of the wind speeds considered.

Wind speed	σ_y / m	σ_z / m
$1 m \cdot s^{-1}$	$0.14\,x^{0.098}$	$0.21\,x^{0.97}$
$1.8 m \cdot s^{-1}$	$0.15\,x^{0.39}$	$0.16\,x^{0.93}$
$2.5 m \cdot s^{-1}$	$0.14\,x^{0.54}$	$0.12\,x^{0.94}$

Equation (2) predict that gas concentrations will be highest very close to the ground, within a few cm. Figure 3 shows a representation of the 3-d concentration distribution for a 1m/s wind speed.

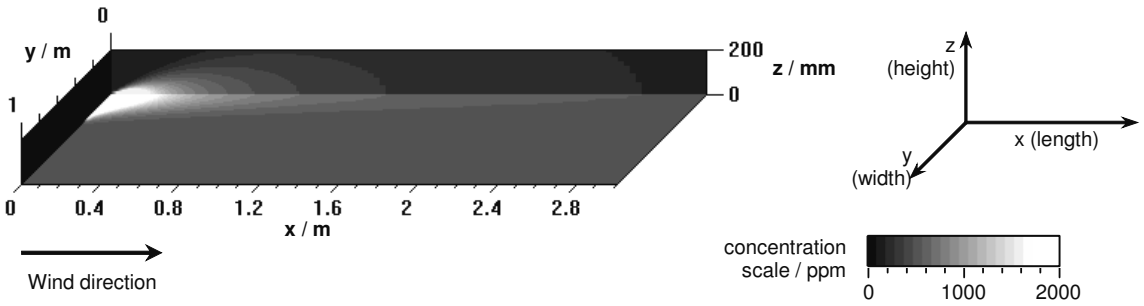

Figure 3. Concentration profile modelled by equation (2), for fitted turbulence conditions, a wind speed of 1 $m \cdot s^{-1}$ and a leak rate of 1 litre min^{-1}.

2.2 Reflectivity model

The ability of the instrument to detect gas depends on the level of instrument noise and the level of backscattered light received by the detector. Because the instrument is self-normalising, information is available on the amount of received light as well as the measured concentration. Thus, the instrument could give a level of confidence in its readings and indicate when a threshold level of light has not been received.

For instrument performance limited entirely by the detector / preamplifier combination, surface reflectivity was considered to be the most significant factor affecting signal to noise ratios, especially for distant targets. We measured the reflectivity of 21 real, flat surfaces encountered in gas leak detection, including brick, concrete, old and new tarmac and bitumen, in wet and dry states. Measurements were made using the same backscatter geometry depicted in Figure 1, at angles of 15º, 45º and 75º to the normal. Figure 4 shows a photograph of the measurement apparatus, based on a near IR diode array spectrometer. We were able to take this apparatus into the field at an early stage in our project to measure a range of real outdoor surfaces.

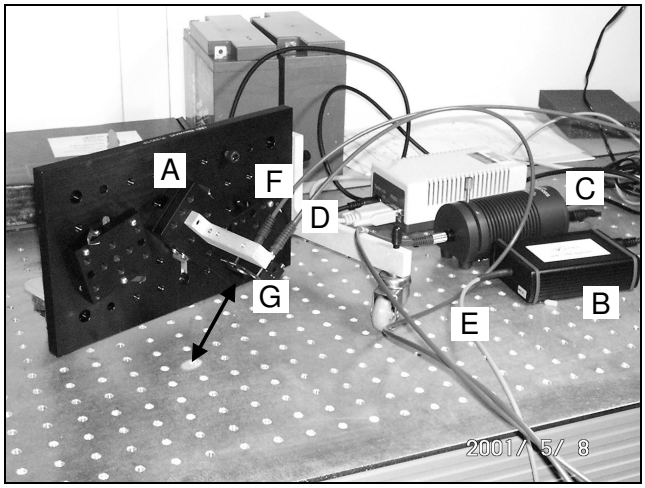

Figure 4. Reflectivity measurement apparatus.

A Optomechanical measurement rig designed to hold the collimating optics for the incident and collected light at three angles of incidence.

B Near infrared diode array spectrometer (Avantes NIR 128) containing a dispersive grating that split the light into its component wavelengths in the range 1100nm – 1750nm, detected at a 128element diode array. Control of the spectrometer and collection of the data was performed using Avantes proprietary software (supplied with the spectrometer) on a lap-top computer. For field measurements, the spectrometer was powered by a 6V lead acid battery via two separate 5V voltage regulators.

C Fibre-aligned tungsten halogen lamp (Avantes) powered from a 12V lead acid battery (two such batteries can be seen in the background of the picture).

D Optical fibre for incident light, diameter 800µm.

E Input fibre to the spectrometer, diameter 300µm. This element was the limiting aperture for the light collection optics.

F Light collection fibre, connected to the short spectrometer input fibre E.

G Input and output collection optics. The measurement spot had a diameter of 9mm and was a distance of 88mm from the collimating lenses.

Measurements were made relative to a diffuse reflection standard (Spectralon) at exactly the same position and height as the target surface. The standard was assumed to have a perfectly Lambertian reflection profile with 99% total reflectivity. Use of the relative standard enabled us to correct for slight changes in the background conditions at the time of measurement.

Readings at different angles of incidence, taken at 1651nm (the operating wavelength of the laser pointer), were fitted to a diffuse reflectance model as follows;

$$\text{returned light power} \quad \delta P_r = P_i \frac{k}{\pi} \rho_{total} (\cos\theta)^{2k} \delta\Omega \tag{3}$$

P_i is the power incident on the surface, which we take to be 10mW. ρ_{total} is the total reflectivity, k is the Minnaert constant[6], θ is the angle of incidence to the normal and Ω is the solid angle of the light collection aperture. The derivation of this equation is given in APPENDIX A, using radiometric relationships defined in reference [7].

The parameters ρ_{total} and k were determined using a least squares fit to our data at the three angles of incidence, with results shown in Table 2, APPENDIX B. Observation of real-world surfaces suggests that in practice, roughness and dirt play an important role in increasing reflectivity at high (>80º) angles of incidence, such that our model may give a worst case estimate of the reflectivity for the most distant targets.

We used the same model to calculate the amount of backscattered light for the laser pointer. The instrument background noise level was found to be constant, giving a signal to noise ratio (SNR) that was proportional to the level of backscattered light collected by the lens[3]. For a returned light power of 20nW the detection limit at SNR=1 was 100ppm.m. Thus we modelled the SNR here as,

$$\text{SNR} = \frac{c}{100\ \text{ppm.m}} \cdot \frac{P_r}{20\ \text{nW}} \tag{4}$$

c is the calculated concentration in ppm.m and P_r is the level of returned light power expected for a 10mW incident beam, scattered from the modelled target distance into a 150mm diameter aperture.

2.3 Combined instrument model

The concentration profile in section 2.1 was used to generate theoretical instrument responses. It was assumed for this exercise that the earth is completely flat and that all target surfaces are horizontal, so for example, walls were not considered. Thus, the angle of incidence is determined by the height that

the pointer is held and the distance to the target; even at moderate distances, the angle to the horizontal is small. The hypothetical instrument response was calculated as follows.

(i) Place theoretical pointer at position P=(x,y,z) in space, relative to the gas leak at (0,0,0).
(ii) Point towards target at position T=(x,y,z), typically on the ground ie with z=0.
(iii) Determine the locus of a line between the two points.
(iv) Calculate the gas concentration at a large number (100) of equally spaced points along this line. For some models a constant set value was added to the value given by equation (2), to account for the methane background.
(v) Use these point concentrations to calculate a numerical approximation to the instrument response in ppm.m for a double pass along the line.
(vi) Plot this response in ppm.m on a map of the ground, at the target location T.
(vii) Plot similar responses to cover all other ground level target locations in a 20m square centred on the pointer.

Note that the gas dispersion model of equation (2) gives infinitely high concentration at the source, since the source is infinitely thin. Such high concentrations were therefore capped at a maximum of 100% volume, to force the calculations to be tractable in the case of a "direct hit" on the leak source. The volume affected by this change was very small, corresponding to around 1cm above ground level. The overall effect might have been to reduce the modelled signal compared to that from an extended source, thus giving a worst case estimate of the line-integrated concentration. In physical terms, this adjustment would model a situation in which, very close to a thin leak source, the passive release model breaks down and the gas has its own momentum, issuing at higher speed under a small pressure differential. It presents a worst case view of the concentration for alternative situations.

The result of this model was a 2-d representation of measured concentrations, mapped to their corresponding ground level targets around the pointer location. The process is illustrated by Figure 5. The exercise was repeated for different pointer locations, modelled wind conditions and background surfaces.

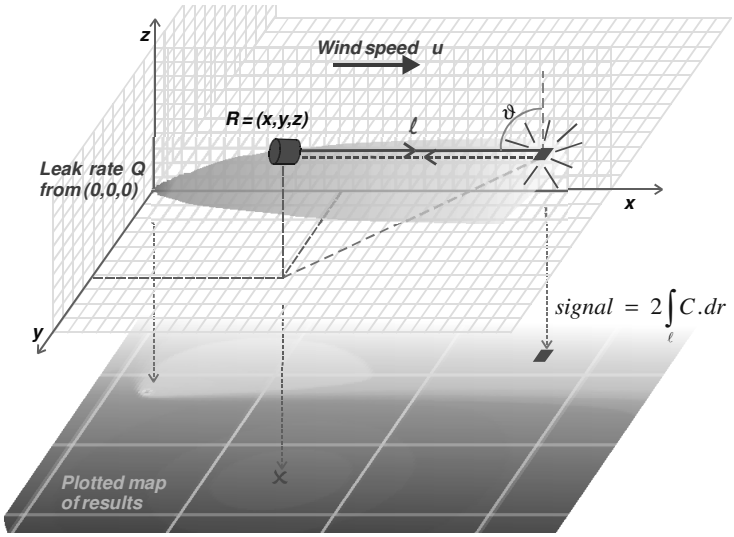

Figure 5. Illustration of combined modelling process

The advantages of numerical modelling were that it provided quick results in controlled circumstances, in contrast to outdoor testing where wind conditions are not repeatable. We were able to investigate trends and consider the questions described later in section 3. However, a number of limitations of this approach should be noted. The gas dispersion model only considered time-averaged probability distributions of gas concentration, not temporal fluctuations. In practice, concentrations are highly variable, especially in urban settings, giving higher peak readings and potentially more rapid dilution of concentration with distance.

3 Results of modelling

We can draw a number of insights from the results, each discussed in the following sections. A theme of this investigation was the issue of whether the results can indicate the location of a gas leak in an intuitive manner for operators more familiar with point measurements.

Unless otherwise indicated, the following standard conditions were used in these models. An intermediate wind speed of u = 1.8 m s^{-1} was used, with a gas leak rate of Q = 1 litre min^{-1}. Results are presented in the same mapped format throughout, with an explanation provided on the first image. In many cases a number of different alternative pointer locations were investigated; because of space constraints we have presented typical indicative examples of these sets of results.

3.1 Ability to zero trace

Determining the absence of gas, or finding out whether there is a gas leak present on site, is a different activity from locating a known leak. A large proportion of public reported escapes can result in a zero trace[8]. We require a zero signal to be a reliable indication of an absence of gas leaks over a given area, therefore the area should be surveyed with sufficient resolution and signal to noise ratio to ensure detection of any significant leaks. A pointer could enable more rapid zero tracing compared to a spot measurement instrument. The following sections discuss a number of potential issues that have been investigated using the model.

3.1.1 Background methane

The background concentration of methane is 1.75ppm [9] but can rise above that in areas close to other methane sources such sewers or cattle farms; for simplicity we used a value of 2ppm. In the absence of a gas leak, the pointer will still measure the background methane, integrated over the interaction pathlength of the laser beam. For long pathlengths, the question was raised of whether this measurement would be interpreted as a spurious gas indication. The issue does not arise for traditional point sampling instruments, since the background level of methane is usually zeroed out in clean air before using the instrument. In the case of the laser pointer, the operator does not know the pathlength nor keep it fixed, and it is not possible to zero out the background reading.

In all cases considered, significant background readings could not be detected within the model with a high enough signal to noise ratio for it to register as a real measurement. At long distances, and therefore grazing angles of incidence on flat ground, there is insufficient returned light to measure anything but signals that are much larger than the background. Figure 6 shows an example in which the background methane can only be detected within a circle around the operator (approx 6m diameter for the “old tarmac” surface), where the signal level is under 30ppm.m, and not elsewhere.

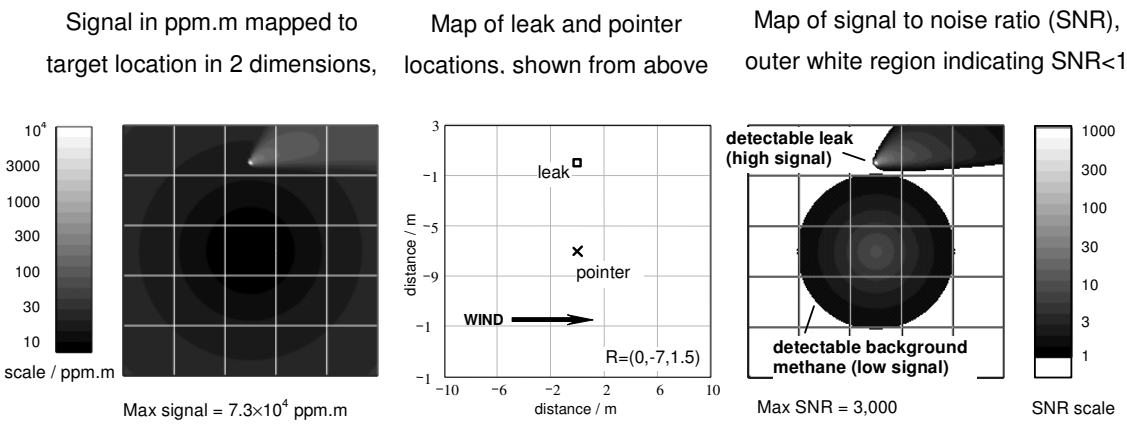

Figure 6. Example set of results showing the effect of the methane background as a detectable but low signal within a circle around the operator, approximately 6m diameter (surface – old tarmac).

However, it is possible that a wall, especially one with a highly reflective surface, might return sufficient light at long distances to enable detection of the methane background. The effect would be counter-intuitive to an operator and would give a false positive indication of a gas leak, which at least would be a fail safe condition, and the spurious signal would reduce on closer inspection.

3.1.2 Target material and range of operation of the instrument

The reflectivity of the target materials and the angle that the laser beam makes with this target both determine the amount of backscattered light collected by the lens, and therefore whether the instrument has sufficient light with which to work. For flat surfaces, the angle to the ground is also determined by the height at which the instrument is held and the distance to the target.

Laser pointers can be designed to fail safe, to give an error if there is insufficient light, so that a false zero trace is not reported. However, we need to ensure the availability of the reading in typical field situations, to justify its use when zero tracing. Our performance target was to be able to detect a signal level of 1000ppm.m at a distance of 10m over flat ground, with a range of target materials. This requirement was tested using the model for various surfaces, and the results are plotted in Figure 7. For this example we chose a pointer height of 1.5m, which is not untypical.

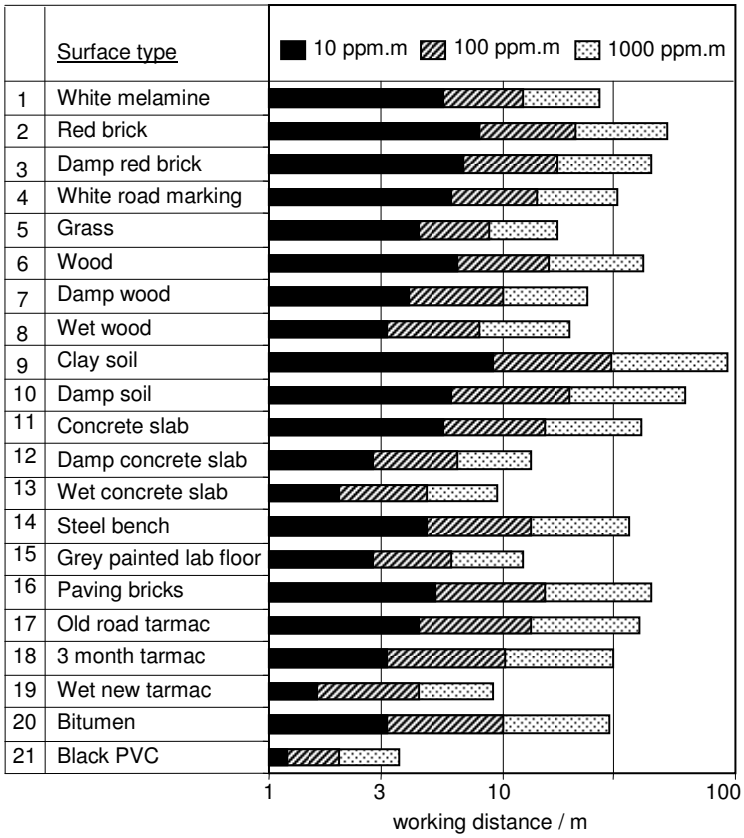

Figure 7. Range in metres at which a hypothetical laser pointer would detect a signal strength of 1000ppm.m, 100ppm.m and 10ppm.m, with a signal to noise ratio of unity, for different surface types. In this model the pointer was held at a height of 1.5m and the target ground was flat.

The results quantify the increased operating range when used over highly reflective backgrounds compared with use over poorly reflective backgrounds. For example, the modelled ranges for clay soil, steel and red brick are well in excess of 30m for large signals, and at 10m signals lower than 100ppm.m are detectable. Black PVC, which has a shiny surface, gave the worst performance but is unlikely to be encountered as a horizontal background, rather as vertical pipework. Wet, new black tarmac (surface type 19) is a worst-case material likely to be encountered more frequently in leak detection operations. For this material, we could detect a 1000ppm.m signal at 9.2m in the model. Or in other words, a zero reading from 9.2m distance over this material would be just capable of indicating that the level of gas was at 1000ppm.m or lower. In fact older tarmac (surface type 17) would be more typically encountered and has better reflectance properties, giving a modelled working distance over flat ground of well over 10m.

3.1.3 Spatial resolution

The fundamental spatial resolution of the instrument is determined by the width of the laser beam. However, we must consider other effects, namely (i) the accuracy with which a user can point the laser beam to the target, and (ii) the resolution required to reliably detect (or show the absence of) a leak. Modelling results suggest that leaks are only detectable within a small target area close to the leak source. The size of the area depends on the distance to the leak, the wind conditions and the surface reflectivity. For this exercise we have used a 1 litre min^{-1} leak in the strongest modelled wind of 2.5 m s^{-1}.

For an old tarmac surface with a pointer-to-leak distance of 10 m, the detectable spot size is small, approximately 80 cm wide in a 2.5 m s^{-1} wind, and extending into an observable plume at greater distances subtending an angle of ±3º at the pointer. The modelled leak is detectable over a width greater than the 10cm width of our modelled source. This is encouraging because in the region corresponding to the source, the passive release model breaks down as previously discussed. The model is also untested here, being based on raw concentration measurements made at downwind distances of greater than 200mm, and made with point sampling detectors that sampled gas from a wider volume than that determined by the source dimensions.

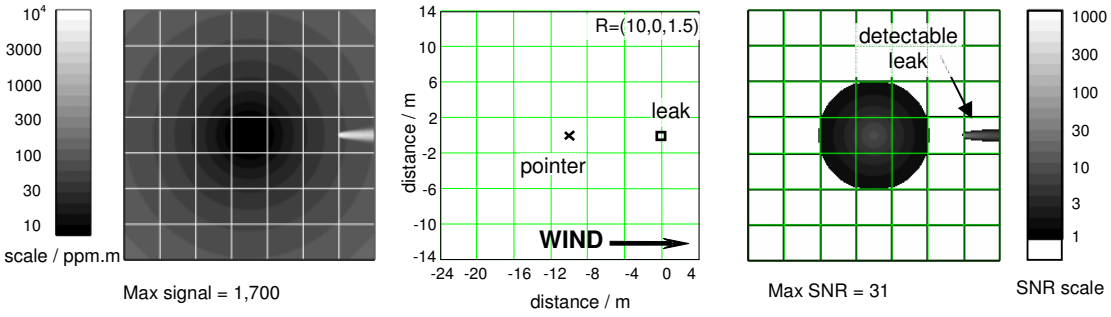

Figure 8. Example of a small detectable spot width at the leak source (see right hand map) at long working distances. The leak can be detected in a 1m wide region, highlighted for clarity.

The model predicts that in the worst case condition, the pointer should be targeted at the leak source, within a tolerance of ±0.4m or better, to yield a detectable gas reading. Pointing the invisible laser beam at 10m distance with this accuracy might be difficult for a user and is likely to require a visual sighting aid and / or visible laser pointer. Furthermore, the laser beam would need to be scanned over the entire surface with just such a high resolution to give a reliable zero trace.

For smaller leaks and / or stronger winds, the required tolerance tightens in our model. In field trials of a prototype pointer instrument, we gained some anecdotal evidence also of the difficulty of detecting very small leaks (unquantified but broadly estimated to be below 0.1 litre min^{-1}) issuing from small (2-3mm) cracks in paving. To detect such small leaks required a direct hit by the laser beam, but this was made difficult at long working distances. We therefore recommend that the laser beam should be expanded as far as possible, so as to just underfill the detectable area created by the photodetector / lens combination.

3.2 Is there potential for ambiguous leak location?

In general, our results show that, in the model at least, the pointer target that gives the largest integrated concentration signal correspond to the location of the gas leak. Such instrument behaviour would be highly intuitive to operators. It derives from the gas dispersion behaviour mentioned previously, that the gas concentration remains highest in a layer very close to ground level, and therefore the line-integrated gas concentration from a higher pointer is dominated by the gas nearest the ground-level target. Some specific questions were raised about whether this principle was sustained in two particular circumstances.

The first question concerned the case of an operator standing within a leaking gas plume. The model has confirmed that a maximum reading would be observed upwind of the operator, corresponding to the leak source. However, a second, broader maximum could also be observed downwind, where increasing interactions lengths coincided with the leak plume. The downwind maximum could be wrongly interpreted as a gas leak source, and confusion could arise particularly if multiple leak sources were present. Figure 9 shows two examples at different distances to the source.

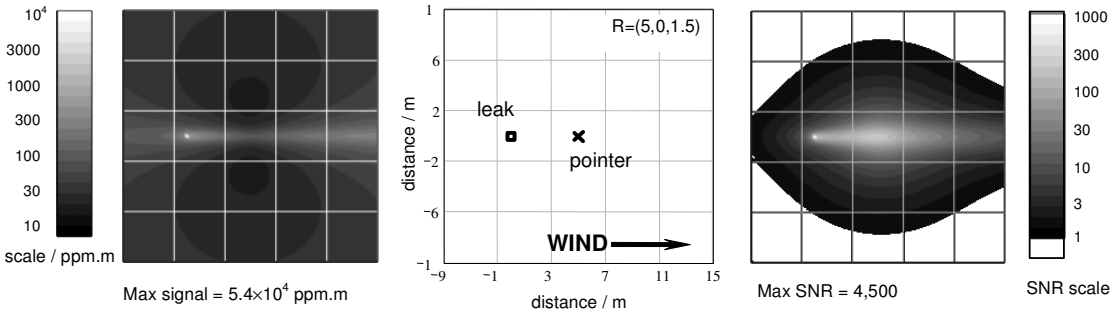

Figure 9(a). 5m away from the leak, a large maximum appears at the leak source with a lower, less well-defined maximum away from the source (surface: dry concrete).

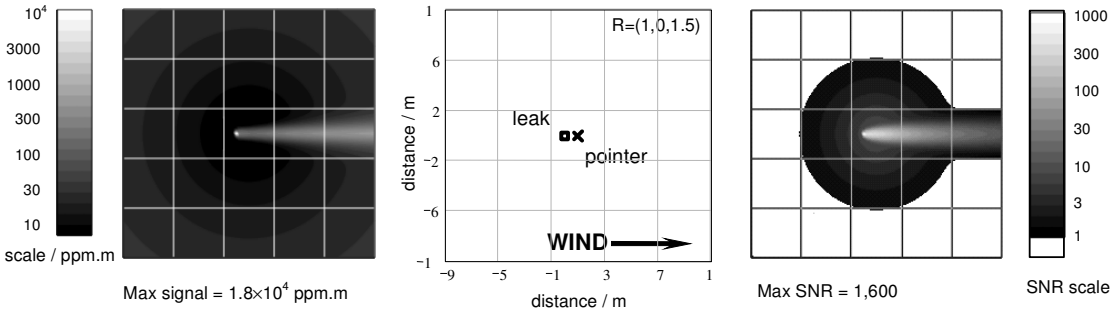

Figure 9(b). Closer to the leak (1m away), the maximum reading from the leak source is reduced, while the maximum away from the leak source has increased.

A number of observations of this case have been made using the model, based on different circumstances. For small leaks (around 1 litre min^{-1}, as used here) and / or poor reflectors, the ambiguity is removed by a poor signal to noise ratio in the region of the broader, smaller apparent maximum reading downwind. The ambiguity is reduced if the pointer is held higher, out of the plume, at > 1m. This has the effect that the interaction distance is defined more by the gas plume height and less by the pointer-target distance.

A further strategy to remove or reduce the ambiguity in the field would draw on operators' existing skills and experience. When using point sampling detectors, it is known that the gas plume drifts downwind and therefore an upwind source is sought for a positive measurement. Knowledge of the wind direction would also be of use in this case with a laser pointer.

The second question concerned the apparent shape of the gas plume. It can be seen that for identical gas leaks, the location of the pointer can distort the apparent plume shape and a gas "shadow" may be observed for plumes viewed from the side. At glancing angles of incidence, the laser beam is more likely to interact with the gas cloud on its way to a more distant target. Figure 10 shows this effect.

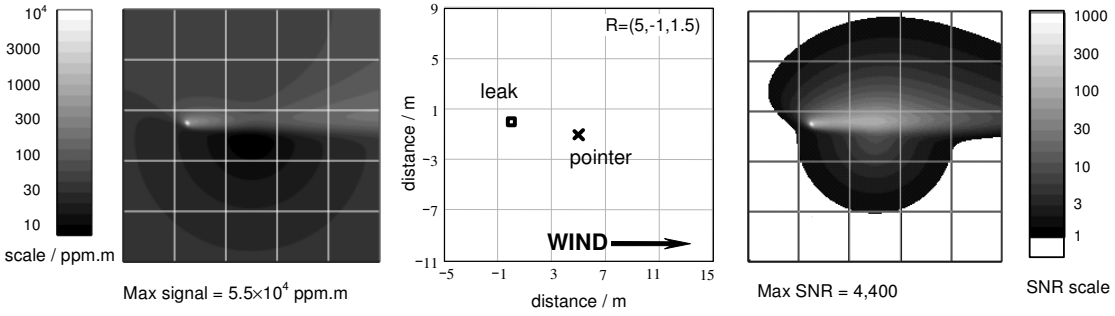

Figure 10(a). With a pointer held at a height of 1m, the gas plume has a little distortion (apart from the previously observed minimum in reading around the operator).

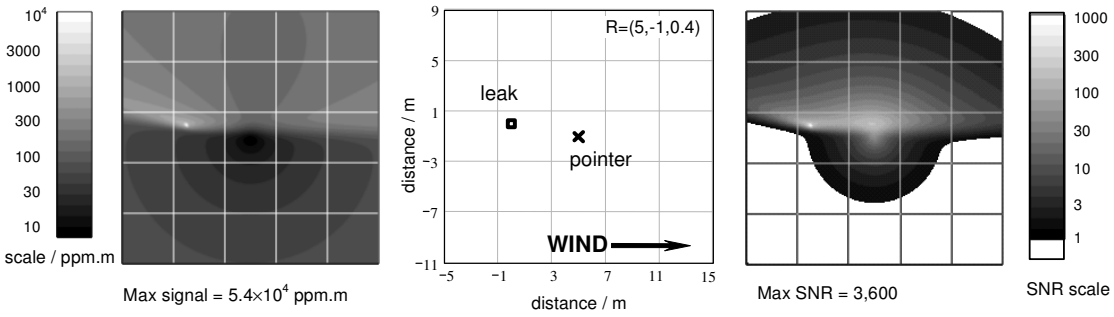

Figure 10(b). With a lowered pointer (at a height of 0.4m) the gas "shadow" has increased (see left hand map of the signal).

Again, for small leaks and / or poor reflectors, signal to noise limitations remove any major ambiguity. The shadowing effect is anyway not considered to be a significant hindrance for leak location, because the plume shape may be distorted but the leak location remains obvious. We can express the effect succinctly as a "gas shadow" behind the leak, which hopefully should convey the nature of the ambiguity to operators.

3.3 What is the optimum pointer height?

We were able to model two competing effects on the instrument response as a function of pointer height. As discussed in section 2.1, gas concentrations remain highest in a layer closest to the ground, within a few cm. Therefore over flat ground, a low pointer will emit a beam at a more grazing angle of incidence, with a greater degree of interaction with the gas plume. However, a higher pointer will gain from better reflectivity at an angle of incidence closer to the normal. So which effect wins?

We modelled pointers used at different heights in a number of different locations relative to the leak source. The maximum modelled signal to noise ratio was used as a figure of merit and has been plotted as a function of pointer height for different pointer / leak positions in Figure 11.

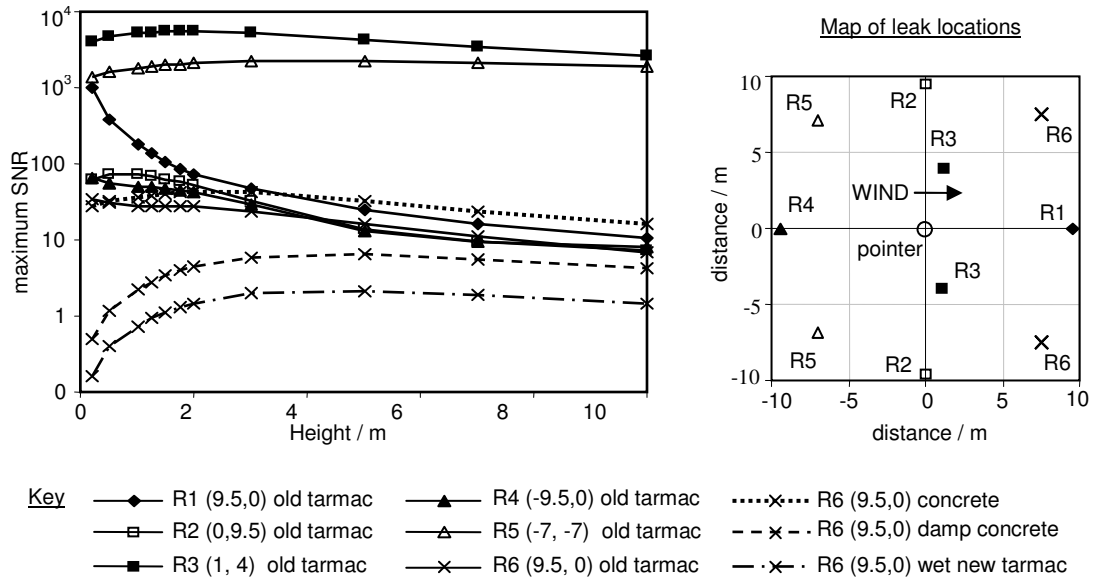

Figure 11. Effect of probe height on the maximum measured signal to noise ratio for a modelled laser pointer operating with a 1litre/min leak in a 1.8m/s wind over a flat surface, at various arbitrarily chosen pointer locations. The map also shows locations that are equivalent by reflection in y=0.

The optimum height depended on the relative location of the pointer and the leak, as well as the target surface. For leaks that were the most difficult to detect, with the lowest observed maximum SNRs, the optimum was rather high for a handheld device and a pointer held at eye level (approx 1.5m or higher) would be preferable to one held at ground level.

4 Instrument field tests

The signal from the laser pointer was compared to the reading from a flame ionisation detector (FID) in an outdoor test with a buried natural gas leak whose leak rate was 10 litre min^{-1}. The FID is a point sampling instrument, whose sample probe was positioned approximately 0.5m downwind of the leak source. The laser pointer was aimed at this same position as a target. Data from both instruments was logged simultaneously, while wind turbulence caused variations in the measured concentration.

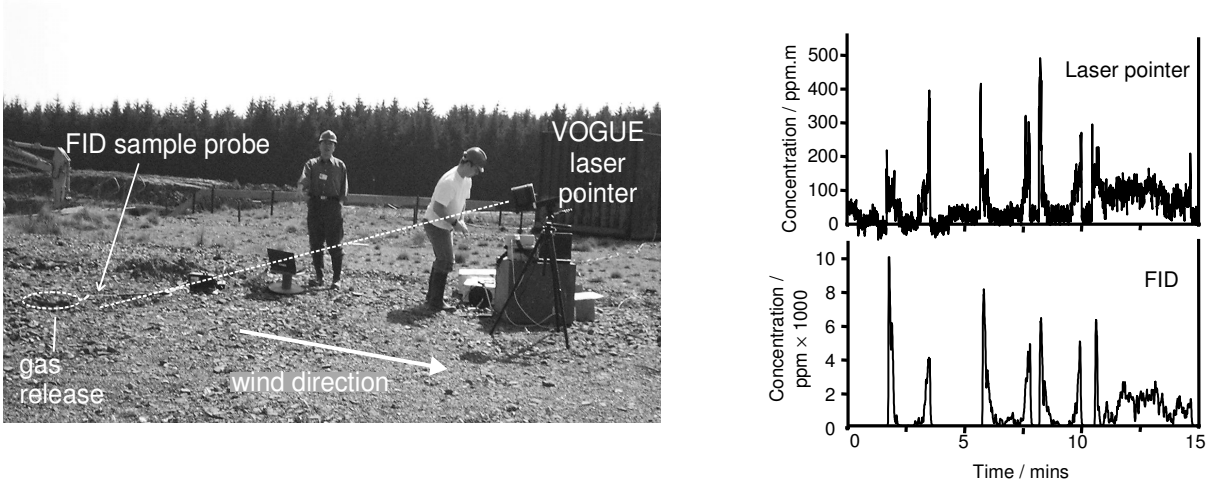

Figure 12. Correspondence between field measurements from a prototype laser pointer and flame ionisation detector targeted at the same sampling location, taken during a release of natural gas at 10 litre min^{-1}.

The results, when re-scaled manually, show a remarkable correspondence between the point sampled readings in ppm and line integrated readings in ppm.m. We suggest that this is again a result of the leaking gas lying very close to ground level. Another related prediction of the model is that the maximum in line-integrated gas concentration should coincide with the location of the gas leak source, and this has also been borne out in field tests.

5 Discussion and conclusions

A model has been developed that combines gas leak dispersion behaviour, reflectivity data and laser pointer performance. Our model represents a simplified and idealised view of reality that has allowed us to quickly study a wide range of trends and phenomena that would have been impossible to quantify in real outdoor tests. We have been able to identify trends and highlight phenomena that help to understand the more complex interaction between real gas leaks plumes and our prototype laser pointer. The model has its limitations and therefore the results should be treated with some caution. However, they have broadly agreed with the general findings of a series of practical field tests of laser pointer prototypes.

The model is limited in a number of ways:

(i) Reflectivity data is limited, being based on a restricted number of measurements taken using equipment that wasn't fully representative of the laser pointer itself. Further work is needed using a prototype pointer to investigate real reflectivities at specific angles of incidence.

(ii) The gas leak model used in this work was non-physical around the leak source, for example giving an infinite gas concentration at the origin. To circumvent this problem, the gas concentration was effectively capped at 100% and the leak source extended to a finite but small volume. During modelling, it has been found that the area around the source has by far the greatest significance for leak detection, but this is where the model is considered most ambiguous and based on limited experimental data.

(iii) The leak dispersion model was constructed for time-averaged gas concentrations as measured in a wind tunnel. However, the temporal variation of real gas concentrations can be very high, depending on wind velocity and turbulence. Thus, much higher concentrations than in the model are occasionally detectable, with better signal to noise ratios.

Despite these potential problems, the modelling work has enabled us to look at trends in performance much more quickly than would have been the case in the field. It has shown us a number of possible effects that are worth investigating and confirming with the real instrument, as follows.

(i) The potential for confusion arising from background methane.

(ii) Possible ambiguities that arise when standing in or near to the leaking gas plume.

(iii) The level of pointing accuracy required for zero tracing.

(iv) The optimum height for use.

For ground based leak sources, the laser pointer measurements appear to be dominated by gas concentrations over a short distance, close to the target surface and to the position sampled by the FID, for both modelled and field results. Maxima in both modelled and field measurements have shown good spatial correspondence to the leak source. This characteristic makes laser pointers potentially intuitive for operators more familiar with point sampling.

6 Acknowledgements

We would like to thank the two organisations who funded this work under EC contract no. NNE5-1999-20031, namely the European Commission and National Grid Transco Plc.

7 References

[1] T. Iseki; H. Tai, K. Kimura, Meas. Sci. Technol. **11** (2000), 594-602.

[2] R.T. Wainner, B.D. Green, M.G. Allen, M.A. White, J. Stafford-Evans, R. Naper. Appl. Phys. B **75** (2002), 249-254.

[3] B. van Well, S. Murray, J. Hodgkinson, R. Pride, R. Strzoda, G. Gibson, M. Padgett, J. Opt. A **7,** (2005) S420-S424.

[4] F.P. Lees, Loss Prevention in the Process Industries, Butterworth-Heinemann, (1996).

[5] J. Hodgkinson, Q. Shan, R. Pride, Environ. Sci. and Technol. (submitted 2005).

[6] M. Minnaert, Astrophys. J. **93** (1941), 403-410.

[7] W.G. Rees, Physical principles of remote sensing, 2nd ed., Cambridge University Press, Cambridge (2001).

[8] Of 1.35 m reported gas UK escapes in 2001, over 259,000 were outside reports, of which around 25% resulted in 'no gas found'. NGT website, http://www.transco.co.uk/safety/index/index.asp, (May 2005).

[9] D.J. Wuebbles, K. Hayhoe, Earth-Sci. Rev. **57** (2002), 177-210.

APPENDIX A. Derivation of reflectivity equation

Iseki et al used the following equation in their model:

$$dP_r = \frac{P_i \rho_{tot} (k+1)}{2\pi} \cos\theta^{2k-1} \, d\Omega \quad \text{W} \tag{5}$$

We realised that this would not normalise successfully for all values of *k,* so for clarity we show a detailed derivation of our equation (3) in this appendix.

Consider a light beam incident on an area δA, as shown in Figure 13. In cylindrical polar coordinates the incident beam has angle θ_i to the normal and rotational angle φ_i about the normal axis. For simplicity, the angle φ has been omitted from the figure, and we assume no dependence on φ.

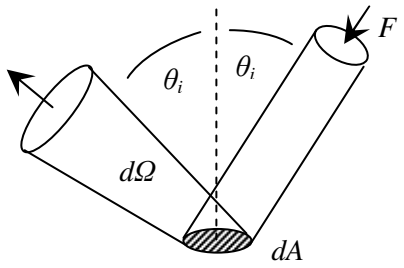

Figure 13. Schematic of terms used to calculate scattered power distribution.

The following radiometric definitions are given by Rees[7]. Let F be the flux density of incoming radiation in W m^{-2}, which is a constant. The irradiance at the surface, E, is given by

$$E = F \cos\theta_i \quad \text{W m}^{-2}. \tag{6}$$

We define $L_r(\theta_r,\varphi_r)$ as the radiance of scattered radiation in the direction (θ_r,φ_r), in W m^{-2} sr^{-1}. the bidirectional reflectance distribution function, BRDF, is then defined as

$$BRDF = \frac{L_r(\theta_r,\varphi_r)}{E} \quad \text{sr}^{-1}. \tag{7}$$

For a Lambertian surface, $BRDF=1/\pi$, but this model was altered by Minnaert who suggested the following relationship[6];

$$BRDF = (\cos\theta_i \cdot \cos\theta_r)^{k-1} \cdot constant \quad \text{sr}^{-1}, \tag{8}$$

where *k* is the so-called Minnaert constant, a parameter that describes non-Lambertian scattering distributions (*k*=1 for a Lambertian surface).

The contribution to power *dI* in direction (θ,φ), into solid angle $d\Omega$, is given by

$$dI \quad = \quad L \cos\theta \; dA \, d\Omega \qquad \mathrm{W}\,, \tag{9}$$

Now we apply these definitions to our system. In this case $\theta_i = \theta_r$, and we can set them both equal to θ for simplicity. At large distances we make a small angle approximation and define dA as the projected cross-sectional area of our laser beam at angle θ, such equation (6) gives;

$$E \quad = \quad F \cos\theta_i \quad = \quad \frac{P_i}{dA} \quad \mathrm{W\,m^{-2}}\,, \tag{10}$$

where P_i is the incident light power in watts. The backscattered radiance from area dA is given by equation (7):

$$L_r \quad = \quad BRDF \cdot E \quad = \quad BRDF \cdot \frac{P_i}{dA} \quad \mathrm{W\,m^{-2}\,sr^{-1}}\,. \tag{11}$$

Now using equations (9) and (11), we find the contribution to the received light power dP_r, assuming that we collect light from the same illuminated area dA (which is true for our system in which the laser beam underfills the detectable area):

$$dP_r \quad = \quad BRDF \cdot P_i \cos\theta \; d\Omega \qquad \mathrm{W}\,, \tag{12}$$

Now substituting from equation (8) gives the following.

$$dP_r \quad = \quad constant \cdot P_i \cos\theta^{2k-1} \; d\Omega \qquad \mathrm{W}\,, \tag{13}$$

The value of the constant is determined by normalisation, invoking a constant ρ_{tot} as the total reflection coefficient, P_r/P_i:

$$\text{total} \quad P_r \quad = constant \cdot \rho_{tot} \; P_i \int_{\theta=0}^{\pi/2} \cos\theta^{2k-1} \cdot 2\pi \sin\theta \; d\theta \qquad \mathrm{W}\,, \tag{14}$$

giving

$$dP_r \quad = \quad \frac{P_i \, \rho_{tot} \, k}{\pi} \cos\theta^{2k-1} \; d\Omega \qquad \mathrm{W}\,. \tag{15}$$

This is slightly different to the equation used by Iseki et al. However, for values of k between values of 0.5 and 2.6 (see Table 2) we found little practical difference between the two equations for the same surface, and both showed a good fit to the experimental data.

APPENDIX B. Reflectivity data

Table 2. Comparison of the reflectivity of different surfaces with a reference. Left hand side: measured relative reflectivity at 1651nm. Right hand side: fitted reflectivity parameters following equation (3).

Material	Measured relative reflectance			Fitted reflectivity parameters		
	Angle to normal (θ)			ρ_{tot}	k	rms fit error / 10^{-3}
	15º	45º	75º			
Spectralon reference	0.99 (by definition)			0.99	1.5	0
White melamine	0.69	0.69	0.51	0.65	1.09	8
Red brick	0.60	0.70	1.12	0.77	0.76	3
Damp red brick	*0.44*	*0.43*	*0.82*	0.54	0.77	10
White road marking	0.59	0.66	0.59	0.62	0.96	13
Grass	0.45	0.34	0.32	0.35	1.26	11
Wood (old rough pine)	0.40	0.43	0.71	0.48	0.79	6
Damp wood	*0.19*	*0.20*	*0.24*	0.21	0.91	0.7
Wet wood	*0.09*	*0.15*	*0.09*	0.12	0.9	10
Soil (clay type)	0.37	0.50	1.32	0.68	0.52	0.2
Damp soil	*0.16*	*0.19*	*0.56*	0.29	0.513	6
Concrete slab	0.27	0.32	0.53	0.36	0.74	2
Damp concrete slab	*0.10*	*0.08*	*0.09*	0.085	1.11	2
Wet concrete slab	*0.06*	*0.05*	*0.03*	0.047	1.24	0.04
Steel bench	0.23	0.069	0.48	0.22	0.70	36
Grey painted lab floor	0.14	0.10	0.12	0.11	1.24	6
Paving bricks	0.13	0.21	0.39	0.23	0.60	6
Old tarmac on road	0.11	0.13	0.31	0.17	0.60	1.5
New tarmac (3 month)	0.065	0.069	0.18	0.097	0.60	2
Wet new tarmac	*0.034*	*0.026*	*0.033*	0.029	1.12	1.3
Bitumen	0.053	0.094	0.16	0.096	0.61	4
Black PVC	0.036	0.013	0.013	0.015	2.60	1.0